A pavement-watering thermal model for SOLENE-microclimat: development and evaluation

Marie-Hélène Azam, Jérémy Bernard, Benjamin Morille, Marjorie Musy, Hervé Andrieu

A pavement-watering thermal model for SOLENE-microclimat: development and evaluation

AZAM Marie-Hélène[a,c,1,*], BERNARD Jérémy[b], MORILLE Benjamin[a], MUSY Marjorie[a,c,1], ANDRIEU Hervé[a,d]

[a] *Institut de Recherche en Sciences et Techniques de la Ville, FR CNRS 2488, F-44000 Nantes, France*
[b] *UMR CNRS 6285, Lab-STICC, F-56000 Vannes, France*
[c] *Cerema, F-44000 Nantes, France*
[d] *Institut français des sciences et technologies des transports, de l'aménagement et des réseaux, F-44000 Bouguenais, France*
[e] *UMR CNRS 6183, GeM, Université de Nantes, F-44000 Nantes, France*

Abstract

In a dense urban area, pavement watering could be a solution to mitigate the Urban Heat Island. For now, mainly experimental studies have been used to evaluate watering techniques. In this study, a soil model dedicated to pavement watering has been developed within the urban climate model SOLENE-Microclimat. This watering model is presented and evaluated via a measurement campaign performed on an asphalt car park during hot days. The measurements campaign reveals that the surface cooling is mainly due to evaporation (80%). However, under warm conditions, the heat flux exchanged between the runoff water and the surface should also be modelled. Indeed, watering events are modelled through a runoff convective heat flux and a latent heat flux. The mean daily RMSE between estimated and observed surface temperature is 1.04^{o}C, 0.86^{o}C, 0.66^{o}C, 0.35^{o}C and 0.21^{o}C

*Corresponding author. E-mail address: marie-helene.azam@cerema.fr Address: Cerema, 9 rue René Viviani, 44000 Nantes, France

respectively at the surface, 5 cm-, 10 cm-, 34 cm- and 50 cm-depths.
Keywords: Pavement-watering, Soil surface temperature,
SOLENE-Microclimat, Urban Heat Island, Climate Adaptation

Highlights

- A watering model is proposed to assess the impact of pavement watering techniques.
- Waterings are modelled through a runoff convective heat flux and a latent heat flux.
- Under warm condition both fluxes should be modelled to reproduce the dynamics.
- Temperature observed at several depths are used to evaluate the computed temperature.

Contents

1. Introduction

The Intergovernmental Panel on Climate Change (IPCC) assessed that heatwaves will be more frequents and more intenses during the 21^{st} century than during the 20^{th} century. The last major European heatwaves led to approximately $70,000$ excess deaths across the continent (Robine et al., 2008 [1]). The urban heat island (hereafter denoted UHI) effect exacerbates the consequences of such climatic event on human health, as confirmed by Laaidi et al. (2012 [2]) and Conti et al. (2005 [3]) who showed a clear relationship between UHI and mortality respectively in Paris and in Italian cities. Reducing the UHI is then a major challenge addressed to the scientist community. Several countermeasures are currently investigated in all regions of the world and under different climates. Santamouris et al. (2016 [4]) performed a review of the performances of the most common UHI mitigation technologies: building material albedo, vegetation, water. He concludes that UHI may be partly or fully annihilated using a combination of all technologies but that there is a need to improve the performances of each of them. The present article focuses on the pavement watering solution. The correct modeling of the physical phenomenon induced by this technique and their interaction with local climate will help to improve its performances.

1.1. Watering techniques

In very dense urban areas, the UHI may be mitigated spreading water over pavements. The evaporation of the water in the air and the heat flux exchanged between the water and the ground contribute to cool both the surface and the air temperature. Under warm conditions, these processes

offer a quick response while the water is spread over the surface. However, the evaporation is constrained by the pavement water-holding capacity (which depends on the surface roughness). Below a certain volume of water spread, all the water is stored in the surface porosity and can evaporate. Above a threshold proper to the surface characteristics, the holding capacity of the surface is overpassed and the water excess streams toward sewers.

Watering techniques have been mainly studied through experimental works (Hendel et al., 2015 [5], Himeno et al., 2010 [6]) which confirm the positive impact of watering technique. Himeno et al., (2010 [6]) found that in the case of hot weather (above 30^oC), pavement watering can reduce the air temperature to 2^oC in the morning and 4^oC in the afternoon. Hendel et al. (2015 [7]) work on the optimization of those waterings, minimizing the total amount of water spread, maximizing the evaporation. With a watering rate of 0.31 to $0.41 L/m^2/h$ every 30 minutes, the surface temperature could be reduced to 4^oC in the morning and 13^oC in the afternoon. According to Broadbent et al. (2017 [8]), the performance assessment of watering techniques during heatwave conditions at the microscale has rarely been modelled. Daniel et al. (2016 [9]), Grossman-Clarke et al. (2010 [10]) and Boadbent et al. (2017 [8]) evaluated the mitigation potential of these techniques at the mesoscale.

1.2. Pavement watering in microclimatic models

In the literature, most of the tools used to simulate the urban surface energy balance, calculate the latent heat flux induced by the vegetation (Grimmond et al., 2010 [11]). However, theirs models are not appropriate for pavement watering application since they do not consider the heat flux

exchanged between the surface and the runoff water.

The Town Energy Balance (TEB) model (Masson, 2000 [12]) is one of the few urban climate models that is able to simulate pavement watering events (Daniel et al., 2016 [9], Broadbent et al. (2017 [8]) at mesoscale. It distinguishes the evapotranspiration from the evaporation over impervious surfaces. In the case of impervious surface, the following processes are modelled: interception, evaporation of the available water and surface runoff. For each surface, a water reservoir is set according to the water holding capacity of the pavement and it content is updated at each time step. It is filled during a watering event and emptied by the evaporation. When the maximum capacity of the reservoir is reached, the excess is transferred to the sewer. By default, the pavement considered in the model is a road and its storage capacity is set at 1mm (Daniel et al., 2016 [9]). However, this parameter is a variable of the model and then may be set to a different value (see section 3.2.1).

The main purpose of this article is to present and evaluate a watering model that has been developed within the SOLENE-Microclimat model. This microclimatic model is a research tool dedicated to urban climate modeling at the neighborhood scale. It consists of several model pieces including a radiative model SOLENE, and several urban surfaces models (buildings, soils, vegetation...) which have been described and assessed in (Malys, 2012 [13]; Musy, 2015 [14]; Bouyer et al., 2011 [15]). In this tool as in most of the microclimate tools (Grimmond et al., 2010 [11]), waterings over impervious surface could not be model.

The watering model is elaborated based on a review of the literature and evaluated on an open asphalt parking lot, chosen to avoid interferences with other surfaces thermal behavior, like solar radiation diffusion and reflection as well as long-wave emission from the surrounding vertical surfaces (building facades). In these conditions, we can isolate the watering model from the other SOLENE-microclimat model pieces and assess it properly. This article is the second step of a complete evaluation of SOLENE-Microclimat soil model. Indeed in a previous article (Azam et al., 2017 [16]), the soil model has been assessed under same conditions.

The model is first presented in section 2. After a review of the different methods used to calculate each heat flux, the equations used in the model are developed and the algorithm is sum-up in a flow-chart (section 2.2.4). In section 3, the model is assessed. The measurement campaign used is first presented (section 3.1). Based on those results assumptions previously made are verified. Results of the model are compared to the observed temperature and heat flux (section 3.2). The model is evaluated on the surface temperature and latent heat flux calculation. Finally, the sensitivity of the model to the soil model node distribution is studied.

2. Method

The proposed watering pavement model will be an additional model pieces to the soil model used in SOLENE-microclimat. The SOLENE-microclimat original soil model is briefly presented in section 2.1 but further details are available in Azam et al.(2017 [16]). Then the proposed watering model is presented in section 2.2.

97 *2.1. SOLENE-microclimat soil model*

98 SOLENE-microclimat soil model is designed for an impervious surface
99 like a pavement coating. Only heat transfer is therefore taken into account,
100 the moisture transfer being neglected. The soil model is defined as a one-
101 dimensional soil column (for each soil facet) where each layer has its own
102 characteristics (Figure 1)

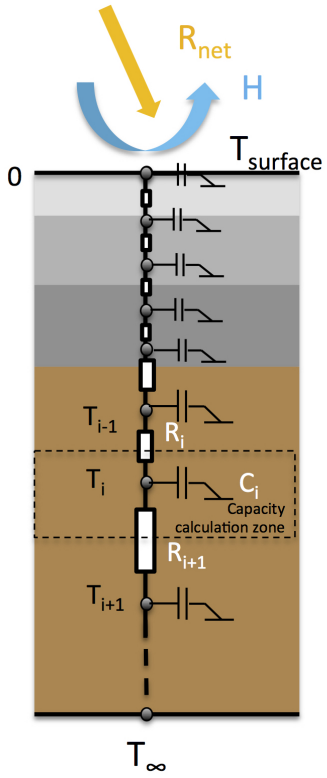

Figure 1: Schematic representation of the soil model: representation of node distribution, heat resistances and capacities, description of a common cross-section of urban soil column with diffusive materials layers in shade of gray and underneath natural soil in brown (Azam et al., 2017 [16])

103 The problem is solved by a finite difference method using an electrical

analogy. A mesh with one node per centimeter is used. At the surface, the upper boundary condition is defined by the surface energy balance detail after. The temperature at 0.75m is set with the measured temperature signal at this depth. A more detailed description of the SOLENE-microclimat soil model can be found in (Azam et al., 2017 [16]).

2.2. Proposed watering model

2.2.1. Energy balance at the surface

The net radiative heat flux density (R_{net}) that reaches a dry pavement is transformed in two fluxes: a conductive heat flux density (Q_{cond}) and a sensible heat flux density (H). Equation (1) is used to define the upper boundary condition of the soil model.

$$R_{net} = Q_{cond} + H \tag{1}$$

R_{net}: net radiative heat flux density $[W/m^2]$
Q_{cond}: conductive heat flux density $[W/m^2]$
H: sensible heat flux density $[W/m^2]$

A watering event alters this energy balance. The water spread on a surface follows one of the following path: 1/ infiltration in the soil, 2/run-off toward the neighboring surface or to the water network and 3/evaporation. Each path implies a modification of the surface energy balance:

- a part of the water infiltrates the soil: the thermal properties of the soil can vary with the water content and a heat flux is exchanged between

the water and the soil layers.

- a part of the water runs-off: a heat flux is exchanged between the water and the surface.
- a part of the water evaporates: a latent heat flux is exchanged between the water and the atmosphere.

Pavement surfaces can be modelled as semi-impervious surfaces (Dupont et al., 2006 [17]) or as impervious surfaces (Herb et al., 2008 [18]; Hendel et al., 2015 [7]). In the first case, downward infiltration should be taken into account whereas the proportion of infiltrated water in the second case is supposed negligible compared with the one that runs-off or evaporates. In this study, we will consider our surface as impervious. Overall the watering model needs to take into account two fluxes initially not considered in Equation (1): a runoff convective heat flux density exchanged between the surface and the water ($Q_{wat-pav}$) and a latent heat flux density (LE) between the water and the atmosphere (Herb et al., 2008 [18]; Hendel et al., 2015 [7]). The resulting surface energy balance is then given by Equation (2). The calculation of these fluxes is further described in the following sections.

$$R_{net} = Q_{cond} + H + Q_{wat-pav} + LE \tag{2}$$

LE: latent heat flux density exchanged between the water and the atmosphere $[W/m^2]$

$Q_{wat-pav}$: runoff convective heat flux density exchanged between the surface and the water $[W/m^2]$

2.2.2. Runoff convective heat flux

Herb et al. (2008 [18]) estimate the convective heat flux exchanged between the surface and the water from the energy absorbed the water and released by the soil. With the same idea, in our model, this runoff convective flux is calculated from the energy absorbed by the water (Equation (3)). The temperature variation is calculated between the soil surface temperature at t and the temperature of the water before it touches the ground. Herb et al. (2008 [18]) model rain events, the water temperature is then supposed equal to the dew-point temperature. In our case, the water spread is suppose equal to the water system temperature.

$$Q_{wat-pav} = \frac{\rho_w.C_{p,w}.h_{w,spr}}{\Delta t}(T_{surf}(t) - T_w) \tag{3}$$

$h_{w,spr}$: water height evenly sprinkled on the surface $[m]$
T_w: temperature of the water $[K]$
ρ_w: water density $[kg/m^3]$
$C_{p,w}$: water specific heat $[J/kg/K]$

Herb et al. (2008 [18]) made the assumption that the runoff water reaches the ground temperature instantly by conduction. The same assumption will be made in the model and verified from the measurements analysis in section 3.1.3.

2.2.3. Latent heat flux between water and atmosphere

The evaporation is driven by two factors: the amount of heat available at the free surface and the vapor pressure gradient in the near air. These

factors depend on meteorological variables including radiation, air pressure, wind speed, temperature but also on other variables like the surface rugosity. Various methods have been developed to evaluate the evaporation rate. Xu and Singh (1997 [19]; 2001 [20]) proposed to sort them into 6 classes: (i) water budget, (ii) mass-transfer or aerodynamic based method, (iii) energy budget method or combination (e.g. Penman, 1948), (iv) radiation, (v) temperature based method, (vi) empirical methods. The empirical methods are applicable for only a limited range of cases or parameters, which makes them not applicable to our case. Singh and Xu (1997 [19]) observed that the water budget methods are based on a simple theoretical basis but that they rarely produce reliable results. The energy budget methods and the combination method reproduce well the physics but they need a considerable amount of meteorological input data. The mass-transfer method is a good compromise since the accuracy is reasonable (Singh and Xu, 1997 [19]) for a less meteorological input data needed. For this reason, it is the method most commonly used by researchers to develop soil models (Asaeda and Ca, 1993 [21]; Qin et al., 2002 [22]; Saito and Simunek, 2009 [23]; Herb et al.,2008 [18], Best, 1998 [24]). It is also used in our model.

The mass-transfer method is based on the Dalton Equation, described by Equation (4).

$$LE = C.[q_{sat}(T_{surf}) - q_a(T_{air})] \tag{4}$$

C: the aerodynamic conductance

$q_{sat}(T_{surf}) - q_a(T_{air})$: the vapor pressure gradient between the actual air va-

por pressure and the saturation vapor pressure at the surface temperature

The aerodynamic conductance is generally modelled using a combination of the air density ρ_{air}, the latent heat L, and a heat transfer resistance R (Equation (5)). Several method can be used to calculate this last parameter. The heat transfer resistance can be calculated as a function of the convective heat transfer coefficient h_c (Mihalakakou et al. 1997 [25]; Herb et al., 2008 [18]); or as a combination of a surface and an aerodynamic resistance calculated using standard Monin-Obukhov similarity theory (Best, 1998 [24]; Asaeda and Ca, 1993 [21]; Qin et al., 2002 [22]; Saito and Simunek, 2009 [23]).

$$C = \rho_{air}.\frac{L}{R} \tag{5}$$

ρ_{air}: air density $[kg/m^3]$

L: the latent heat $[J/kg]$

R: heat transfer resistance's $[s/m]$

In our model, the heat transfer resistance is a function of the convective heat transfer coefficient (Equation (6)). It is calculated from the correlation method with a characteristic length of 1m (for more detail see Azam et al., 2017 [16]). This method considers forced, mixed and natural convection.

$$R = \rho_{air}.\frac{C_{p,air}}{h_c} \tag{6}$$

$C_{p,air}$: air specific heat $[J/kg/K]$

h_c: the convective heat transfer coefficient $[W/m^2/K]$

As the surface is impervious, the latent heat flux is only calculated when some water is present on the surface. This heat flux depends on the air characteristics (temperature, pressure, humidity and wind speed). The vapor pressure gradient is calculated between the air at a certain height and the saturated air very close to the water surface. The hypothesis is made that the saturated air very close to the water surface is at the same temperature than the water surface. The vapor pressure is calculated according to the Magnus-Tetens formulas (Alduchov and Eskridge, 1996 [26]) described by Equations (7), (8) and (9).

$$q_{sat} = 0.662 \, \frac{VP_{sat}}{101325 - 0.378 \, VP_{sat}} \tag{7}$$

$$q_a = 0.662 \, \frac{VP_{sat} \frac{RH}{100}}{101325 - 0.378 \, VP_{sat} \frac{RH}{100}} \tag{8}$$

$$VP_{sat} = 611.2 \, exp(\frac{17.67 \, T}{243.5 + T}) \tag{9}$$

VP_{sat}: saturated vapor pressure $[Pa]$

RH: Relative Humidity $[\%]$

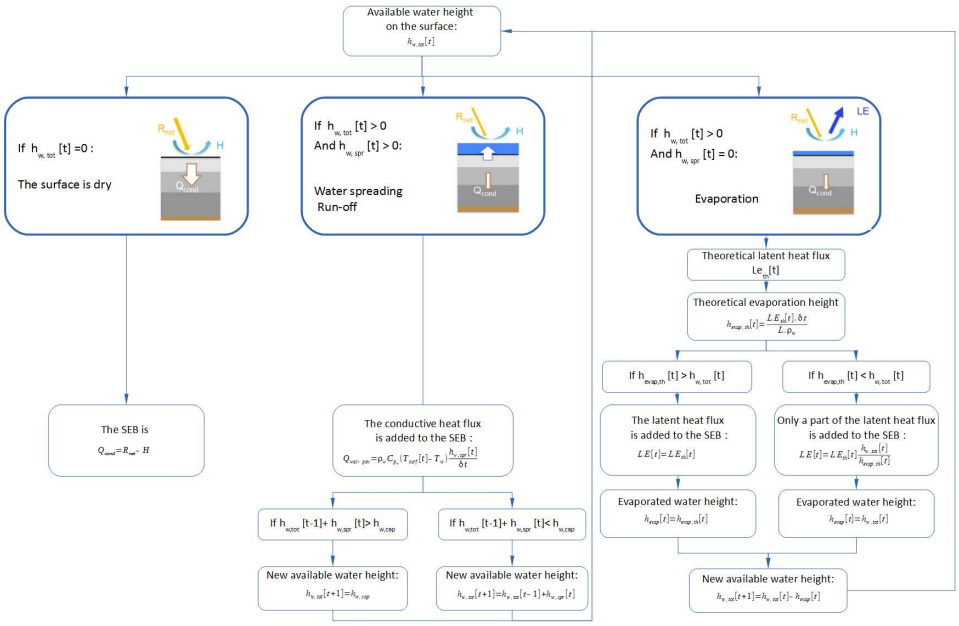

Figure 2: Flowchart of the surface energy balance calculation process for each step of a watering event.

2.2.4. Heat fluxes dynamic

The Surface Energy Balance (hereafter denoted SEB) method is presented Figure 2. For each time step, the equivalent height of water that is evenly sprinkled on the surface is noted $h_{w,spr}$. The total height of water is noted $h_{w,tot}$. Then three cases are considered:

- $h_{w,tot}$ is equal to 0,
- $h_{w,tot}$ is higher than 0 and $h_{w,spr}$ is higher than 0,
- or $h_{w,tot}$ is higher than 0 but $h_{w,spr}$ is equal to 0.

In the first case, the surface is dry then the conduction flux is simply defined as the difference between the global radiation flux and the sensible heat

flux. In the second case, water is sprinkled on the surface. We assume that no evaporation occurs at this time step. The energy is exchanged between the water and the ground. This convective heat flux is calculated considering that the additional height of water $h_{w,spr}$ reaches directly the surface temperature. Then a proportion of the total water height runs off decreasing the height of the water layer. The height $h_{w,cap}$ of the water layer that remains at the surface depends on the water-holding capacity of the pavement. In the third case, the sprinklers are off some water remains on the surface. Only evaporation occurs and its potential is estimated and converted into an equivalent water height $h_{evap,th}$. If $h_{w,tot}$ is higher than $h_{evap,th}$, the latent heat flux is equal to the evaporation potential. Else, the remaining height $h_{w,tot}$ is converted to an equivalent latent heat flux. The water height decrease is equal to the evaporated water height. Then the next time step is considered.

3. Model assessment

The model is evaluated an open asphalt parking lot. The measurement campaign and the analysis of the watering event will be first presented (section 3.1). Then the model will be applied to this case and assessed (section 3.2).

3.1. The campaign and the data

3.1.1. Studied area and measurement description

Data from the ROSURE/HydroVille experiment (Cohard et al., 2017 [27]) are used to calibrate and evaluate the pavement watering model. The

experiment site is located near Nantes (France) and consisted of an asphalt car park of $2500m^2$. This campaign especially focused on surface and air temperatures and on heat flux measurement during a warm summer period (June 2004). During this experiment, the car park was watered by means of a set of artificial rain events (Figure 4).

Figure 3: View of the experimental site during a watering event (an asphalt parking lot of $2500m^2$)

Throughout the observations available for this campaign, this study focused on the following variables, all observed in the middle of the car park:

- surface and ground temperature: vertical profile at 0, 1, 2, 3, 4, 5, 6, 10, 15, 24, 34, 50 and 75 cm depth;
- wind speed and direction;
- convective heat flux;
- latent heat flux;

- radiation components.

The humidity and air temperature was measured outside from the car park. The equipment used and their position is given in Figure 4. The data were collected with a 1 min time step except for the sonic anemometer and the KH20 Campbell Sci whose time step were 0.1 s. The final data were averaged to 15 min time step.

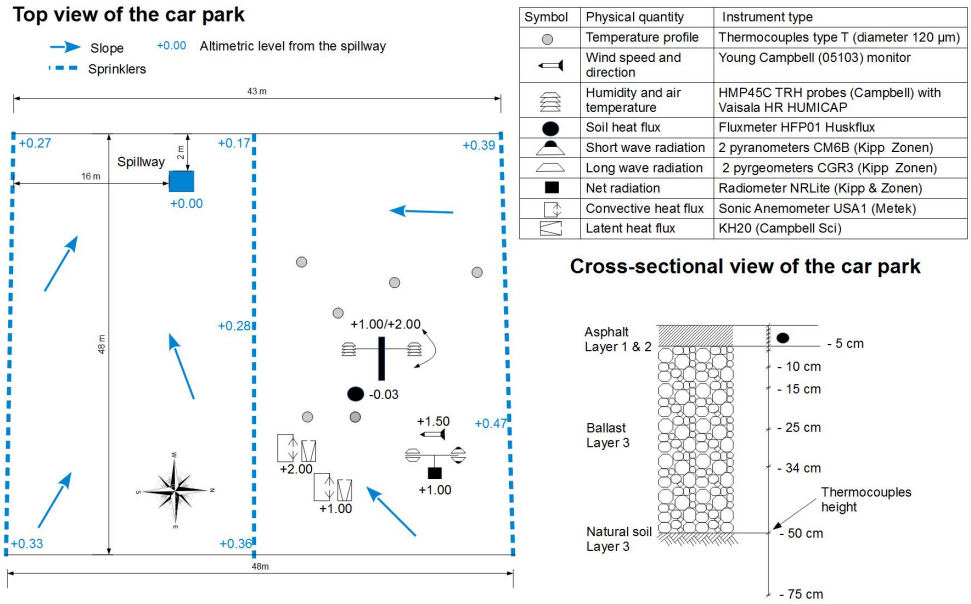

Figure 4: Top view of the car park with instruments approximate location during the campaign and cross-section of the soil composition (see Table 3 for the material properties)

3.1.2. Description of the watering events

16 watering events (including one natural event - the 15^{th}) were recorded during the entire measurement period (Figure 4). Each of them is described

Watering Number	**Date** DD/MM/YY HH:MM	**Time** minutes	**Total vol. of water** m^3	**Intensity** mm/m^2	**Flow** m^3/h
1∗	02/06/04 13:42	20	16.96	6.78	43
2∗	03/06/04 09:53	20	13.08	5.32	43
3∗	03/06/04 15:04	20	15.05	6.02	44
4	04/06/04 08:49	3	2.04	0.81	44
5	04/06/04 11:57	1.5	1.12	0.45	44
6∗	04/06/04 13:57	17	14.92	5.97	44
7	07/06/04 08:51	20	13.75	5.50	42
8	07/06/04 13:43	30	21.33	8.53	44
9	08/06/04 09:45	19	12.40	4.96	44
10	08/06/04 15:04	5	3.06	1.22	38
11	09/06/04 09:25	20	14.10	5.64	42
12	09/06/04 13:40	20	16.25	6.50	46
13	09/06/04 15:38	2	1.60	0.64	48
14	10/06/04 08:30	20	15.44	6.18	45
15	10/06/04 12:25	28	2.95	1.18	-
16	11/06/04 08:40	2	1.66	0.67	43

Table 1: Description of each watering event

in table 1. During the events numbered 1,2,3 and 6, some technical issues occurred and the total volume of water may be different from what is presented in Table 1. For each event, several parameters have been measured:

- inlet: water temperature, flow, and volume,
- outlet water temperature, flow, and volume,
- duration of each watering.

An indication is given on the approximate duration of the drying periods.

3.1.3. Consistency of the heat fluxes dynamics with the model assumptions

Sections 2.2.2 and 2.2.4, the assumption was made that energy is exchanged between the runoff water and the surface only during the first time

step (t=15 minutes). Then the latent heat flux is modelled. Those assumptions are here verified analysing the temperatures and heat flux measurements.

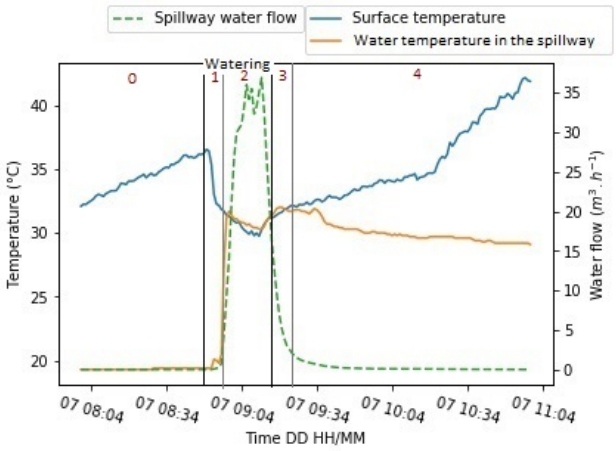

Figure 5: Watering event number 7, June 07^th at 08:51am, measured surface temperature in the center of the parking lot and measured water temperature and water flow in the spillway

The surface temperature evolution is compared to the water temperature and flow in the spillway in Figure 5. As soon as the watering event begins (black line on Figure 5), the surface temperature drops and the water temperature increases (zone 1 on Figure 5) until they reach a balance (grey line on Figure 5). A delay of several minutes can be observed between the temperature signals and the water flow signals (zone 1 and 3 on Figure 5). The thermocouples are located at several meters from the spillway, as it can be observed in Figure 4. The delay between the different signal is consistent with the water travel time between the thermocouples location and the spillway. As the balance is reached, both temperatures increase (phase 3): no

more energy is exchanged between the surface and the water layer. As soon as the water flow decreases (green plot), all the water has been drained. The thermocouple now measures the temperature of the standing water in the spillway, which slowly decreases (zone 4 on Figure 5).

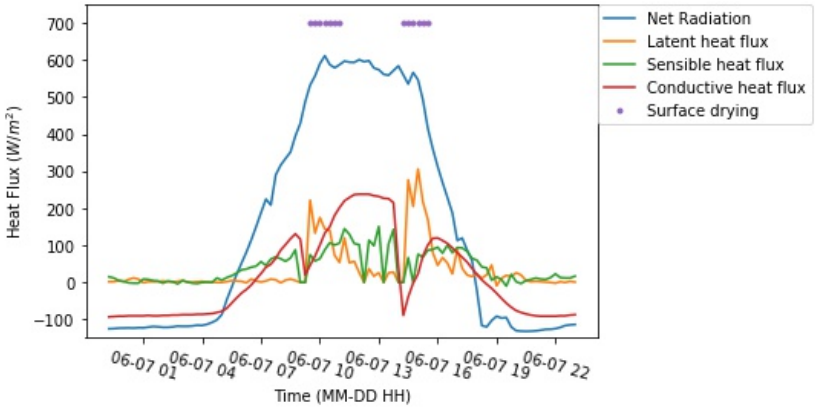

Figure 6: Observed surface energy balance (June 07^th)

Those observations can be confronted with the heat fluxes measured presented in Figure 6. As said before the water temperature reaches very quickly (less than 20 minutes) the surface temperature (Figure 5) whereas the conductive heat flux in the ground has a decreasing peak right after watering which then shrink in a short time (about one hour) (Figure 6). Cohard et al (2017 [27]) also noticed a similar trend: the heat flux transferred from the ground to the water can reach $438W/m^2$ during a watering event and decreases as soon as the sprinklers stop (15 minutes). Those observations are consistent with the assumptions made for our modelling as well as the one used by Herb et al. (2008 [18]): the run off convective heat flux exchanged between the water and the surface can be attributed to the first time step of the watering event. We assumed that air was saturated during the wa-

tering process and no evaporation occurred immediately. This assumption could not be verified in this measurement campaign since the latent heat flux sensor was protected when the sprinklers were working.

3.1.4. Water budget

When some water is spread over a surface, a fraction runs off whereas the other fraction is intercepted by the surface until evaporation or infiltration. The distribution of runoff and pavement storage depends on the surface water-holding capacity, itself related to the surface roughness. This characteristic is a parameter of the model that should be set by the user. The purpose of this part is to get an estimation of this parameter through the measurements of the water budget.

Cohard et al. (2017 [27]) estimated that for each watering event, a maximum 0.1 and 0.2 mm of the height spread water infiltrates the ground. The water left over the surface is thus considered as entirely evaporated. To calculate the corresponding amount, they tested several methods derived from latent heat flux measurement or estimation. Their conclusion is that the latent heat flux estimated according to the SEB method (using measurements for the other fluxes values) was the most accurate. The results fitted with the water budget contrary to the other method used. They were then able to evaluate for each watering event the amount of water evaporated. For events with high volume of water (more than 2 mm), the mean evaporated height is 0.7mm. This value will be used as reference data for the evaluation of the model, and the water holding capacity will be calibrated in the model (see section 3.2.1).

Surface energy balance heat flux	**Input data used to calculate each flux**
Convective heat flux	wind speed
	air temperature*
Net radiative heat flux	Net radiative flux
Latent heat flux	water height
	water-holding capacity of the surface
	air relative humidity*
	air temperature*
Runoff convective heat flux	water temperature
	total sprinkled water for each event

*measured outside from the watered zone of the car park

Table 2: Detail of each input data necessary to calculate the upper boundary condition.

3.2. Comparison between simulation and measurement

The model ability to properly reproduce the physical phenomenon related to a watering event is evaluated in this section. The model setup used are first presented, then the model is evaluated at several depths. Finally, as the soil model is proposed for different optimized grid distribution, the model sensitivity to the node distribution is studied.

3.2.1. Model setup

The simulation is run for the whole period from June 5^th, 00:00 to June 14^th, 00:00, with a time step of 15 minutes. For the soil thermal model, a centimetric grid is used.

Surface energy balance:

The heat fluxes are calculated from the observed data presented in Table 2. The convective heat flux is calculated from the air temperature and the wind speed. Radiative heat fluxes are the observations. The latent

and run-off convective heat fluxes are calculated according to the processing chain presented Figure 2. The runoff convective heat flux is calculated using the amount of water sprinkled during each watering event derived from the measurement. The temperature of the sprinkled water is set at 18^oC before touching the ground. The latent heat flux is calculated from the air characteristics measured outside from the watered zone.

Thermal characteristics:

The soil is composed of three different materials: $5cm$-of asphalt, $45cm$-of ballast and an altered mica-schist natural soil underneath. Soil composition and thermal properties have not been measured during the campaign. They have been calibrated according to the observed soil thermal profile, reducing the difference between the measured and simulated surface temperature, with a centimetric-grid. Data acquired on the 6^{th} of June is used for calibration. From the measured temperature gradient, changes in the soil thermal properties within the first layer were identified (0–1 cm, 1–5 cm). Values are gathered in Table 3.

Layer	**Material**	**Depth**	**Thermal conductivity**	**Volumetric heat capacity**
Number	Characteristics	m	$W.m^{-1}.K^{-1}$	$10^6 J.m^{-3}.K^{-1}$
0	Asphalt Concrete	0.01	2.5	2.3
1	Asphalt Concrete	0.05	2.5	2.1
2	Old Filled Ballast	0.5	1.8	2.3
3	Altered Mica-schist Natural Soil	1	1.3	2.1

Table 3: Calibrated characteristics of the soil

380 **Water-holding capacity:**

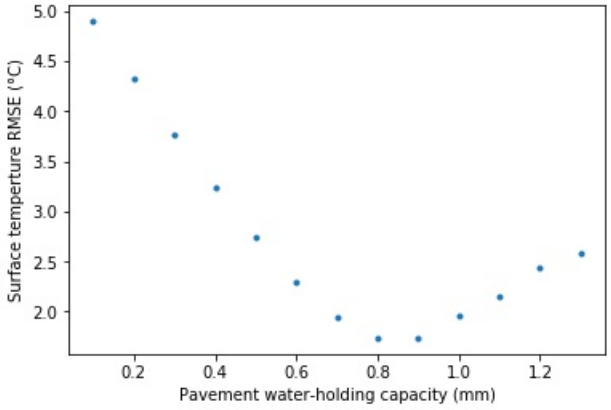

Figure 7: Surface temperature RMSE as a function of the pavement water-holding capacity (mm) for the calibration period (June, 7^{th}, and 8^{th})

381

382 The water storage capacity of the surface may vary a lot depending on
383 the surface type. To better evaluate this value for our studied area, the
384 model has been run for two days from the 7^{th} to the 8^{th} of June (4 watering
385 events), testing the water storage height from 0.3 to 1.4. The effect on the
386 temperature surface RMSE is shown Figure 7. A water holding capacity of
387 0.8 mm minimizes the surface temperature RMSE and then is used for the
388 studied car park surface. Figure 8 presents the results of the calibration
389 period and a minimum for a height of 0.8mm. The temporal variations are
390 well reproduced (there is no phase lag between the signals) except during the
391 watering events.

392 This value is consistent with mean evaporated height calculated from SEB
393 method for a high amount of water (0.7 mm). In the literature Hendel et al.

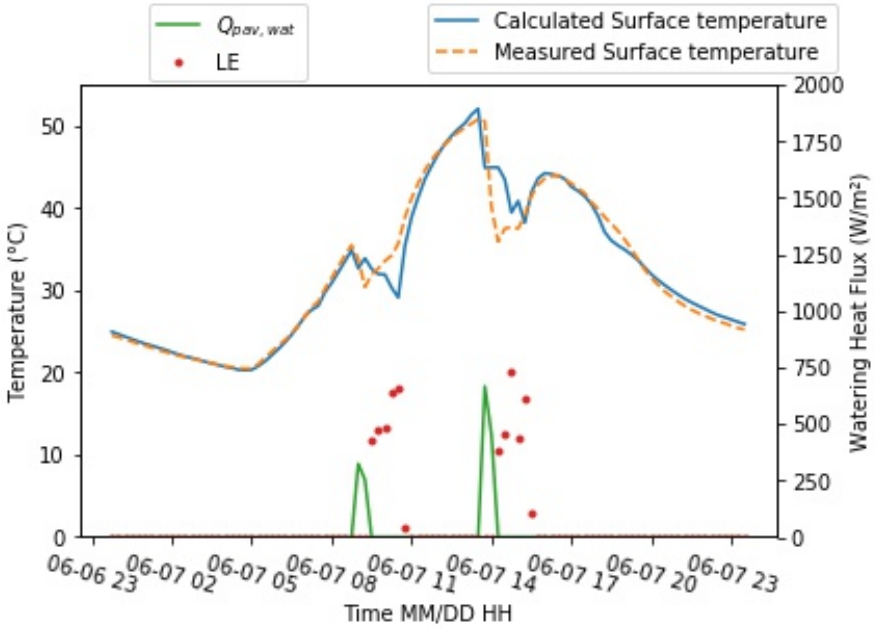

Figure 8: Comparison of simulated and measured temperatures at the surface for the calibration period (June, 7^{th}, and 8^{th})

(2015 [7]) estimate to 1mm the water holding capacity of road surface in the center of Paris. In TEB the default value is also set to 1 mm (Daniel et al., 2016 [9]).

3.2.2. Watering model evaluation on ROSURE data

This paragraph deals with the evaluation of the model which is performed by comparing the time series of observed and modelled surface temperatures (Figure 9). Over the all data set, the temporal variations are well reproduced (there is no phase lag between the signals) except during the watering events. The same shape is obtained (a decreasing peak followed by more steady period and then an increasing peak) but a lag is observed. This lag might

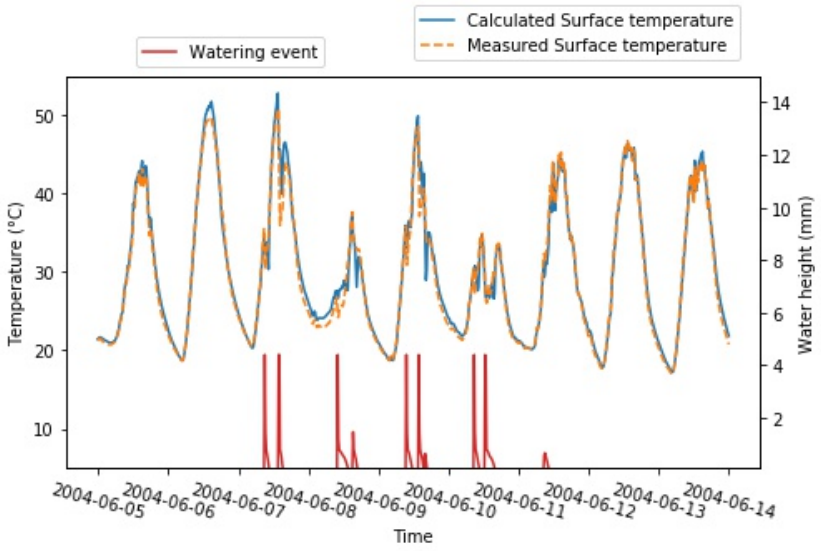

Figure 9: Comparison of simulated and measured temperatures at the surface from June, 5^{th}, to 13^{th}

have been attributed to the assumption that the drying stage does not start as long as the sprinklers are in operation. To verify this assumption, we have run some simulations starting the evaporation stage while sprinklers were still working. The same temporal lag was noted and the simulated surface temperature was lower than the observed one or the initial simulation. This lag error could be attributed to the relative humidity measurement used for the latent heat flux calculation. The sensor is located outside from the sprinkled area and thus potentially underestimates the real relative humidity of the air in the watered area. This results in an overestimation of the latent heat flux which may affect the dynamic of the surface energy balance.

In order to determine the overall model performance, the RMSE between estimated and observed temperatures is calculated at the surface and at sev-

Depth	**RMSE** (^{o}C) From June 8^{th} 23:45 to the 13^{th} 23:45 (soil + watering model)	**RMSE** (^{o}C) From June 11^{th} 23:45 and 13^{th} 23:45 (soil model only)
Surface	1.04	0.71
5 cm	0.86	0.93
10 cm	0.66	0.78
34 cm	0.35	0.46
50 cm	0.21	0.29

Table 4: Evaluation of the centimetric grid watering model according to the experimental data

eral depths. To estimate the error which may be attributed only to the watering model, the RMSE is calculated for two different periods. The first period includes the entire campaign without the calibration days (from June 9^{th} to June 13^{th}), whereas the second includes only two dry days (June 12^{th} and 13^{th}). The first set of RMSE assesses the overall model performance (soil and watering models) while the second RMSE set indicates the performance relative to the soil model only (ability to reproduce heat transfers into the ground). Results are presented in Table 4. The absolute RMSE for the surface temperature is larger when watering events are simulated (1.04^{o}C) than when only the soil model is needed (0.71^{o}C). For this specific dataset, the watering model increased the soil model error of 46%. As the simulated days are not similar (weather condition are varying), this value is only representative for this specific simulation.

The assumption was made that the water-holding capacity of the surface was $0.8mm$. As it is an important parameter, the model is also evaluated on its ability to calculate the latent heat flux. For each event, the latent heat

Watering	**Date**	**Duration**	**Total height of the water layer spread**	**Latent heat measured from SEB method**	**Latent heat calculated by the model**	**Relative error**
Number	DD/MM/YY HH:MM	minutes	mm	$10^6 J$	$10^6 J$	%
7	07/06/04 08:51	20	5.50	2.11	1.96	-7.17
8	07/06/04 13:43	30	8.53	2.36	1.96	-17.04
9	08/06/04 09:45	19	4.96	2.00	1.96	-2.12
10	08/06/04 15:04	5	1.22	1.52	1.96	28.71
11	09/06/04 09:25	20	5.64	1.52	1.96	28.79
12	09/06/04 13:40	20	6.50	1.42	1.76	23.77
13	09/06/04 15:38	2	0.64	1.30	1.57	21.07
14	10/06/04 08:30	20	6.18	1.72	1.96	13.66
15	10/06/04 12:25	28	1.18	1.74	1.96	12.60
16	11/06/04 08:40	2	0.66	1.32	1.63	22.88

Table 5: Comparison of the latent heat flux estimated from SEB residue and calculated by the model. For each event, the latent heat fluxes are summed over the event duration.

fluxes calculated by the model and estimated from the SEB residual method are integrated over each event. The total energy due to evaporation for both methods is compared in table 5. The relative error stays below 29%. On average, the model overestimates the latent heat flux by 12%.

The air temperature and the relative humidity used to calculate the evaporation were measured outside from the car park. If local parameters were used, an increase of the relative humidity and a decrease of the air temperature would have been observed. Then the calculated evaporation heat flux would have been smaller. The use of nonlocal meteorological data overestimates the latent heat flux calculation.

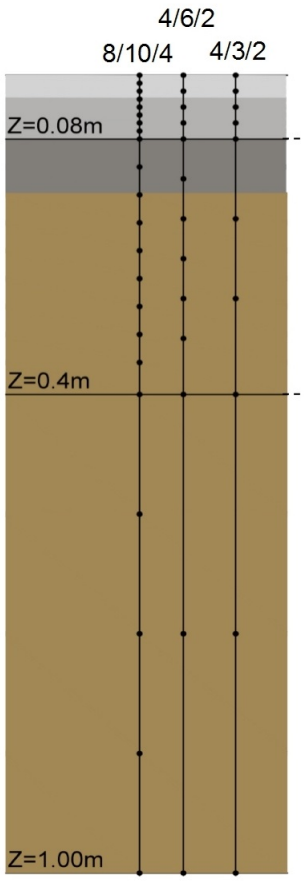

Figure 10: Description of the different grids

3.2.3. Model's sensitivity to the discretization

In order to reduce the simulation duration while keeping a reasonable accuracy, three node distributions for the soil layer have been proposed in Azam et al. (2017 [16]). They are presented in Figure 10. The sensitivity of the model to this nodes distribution is here evaluated.

Figure 11 compares the surface temperature modelled with the three different node distribution with the measured one. Firstly, the three node distri-

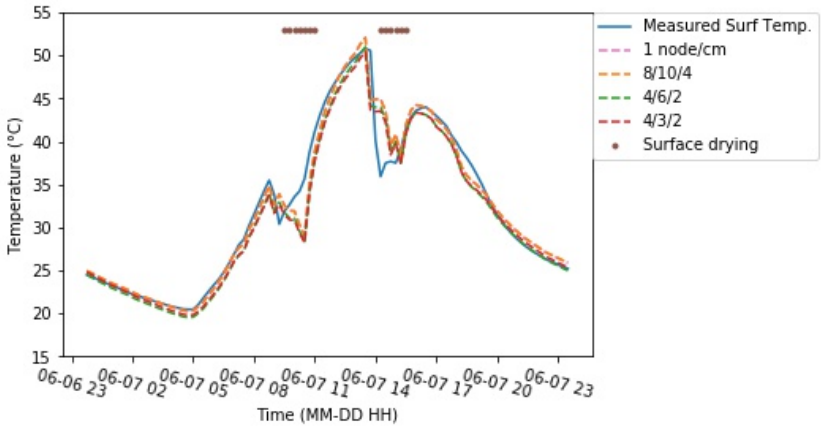

Figure 11: Surface temperature calculated with the different grids compared to that measured (June 7^{th})

butions allow an accurate modelling of the time series of surface temperature. Nevertheless, the daily maximum and minimum peak are underestimated.

The underestimated daily maximum peak and minimum trough are due to the heat fluxes implementation during watering events. However, the reduction in the number of nodes deteriorates the results as it leads to deteriorate the representation of the heat transfer into the ground. In fact, this induces a time shift of heat conduction, the main influence of which appears when its sign changes.

The RMSE between simulated and observed surface temperatures is calculated for each node distribution (Table 6). The accuracy loss due to the reduction of the number of nodes is also evaluated calculating the RMSE of the simulated surface temperature between each node distribution and the centimetric grid (1 node per cm). The 8/10/4 grid has almost no effect on the simulation performances (the RMSE increase is lower than 4%). The

Date	**Reference data for RMSE calculation**	**centimetric grid**	**grid 8/10/4**	**grid 4/6/2**	**grid 4/3/2**
From June 8th 23:45 to the 13th 23:45	observed temperature(^{o}C)	1.04	1.04	1.44	1.50
(soil + watering model)	simulated temperature using centimetric grid (^{o}C)	-	0.02	1.18	1.21
June 12th and 13th	observed temperature (^{o}C)	0.70	0.72	1.10	1.20
(soil model only)	simulated temperature using centimetric grid (^{o}C)	-	0.03	1.14	1.15

Table 6: Evaluation of the model with a reduced number of nodes

absolute RMSE increase due to the node distribution is almost similar regardless the models used (soil model only or soil model + watering model): 0.02, 1.18, and 1.21 ^{o}C respectively for grids 8/10/4, 4/6/2 and 4/3/2. If we report these RMSE to the one due to the model itself (centimetric grid relative to the observed data), the relative accuracy loss due to the nodes distribution is much lower when the water model is taken into consideration.

4. Conclusion

This article focuses on pavement watering as a possible mitigation technique of the UHI effect under heat waves conditions. The literature review revealed that it technique has been mainly studied through experimental works. To the best of our knowledge, the impact of pavement watering on urban energy balance at the microscale has not yet been addressed by modelling.

The main purpose of this article was to implement a watering model within an urban microscale model (SOLENE-Microclimat) and to evaluate it according to an observation campaign.

The watering model was elaborated on a literature review and evaluated on an open asphalt car park. Two fluxes were taken into account: the runoff convective heat flux (exchanged between the surface and the runoff water) and the latent heat flux. The runoff convective heat flux is often neglected by existing models at mesoscale whereas the high difference of temperature between surface and the water spread makes it prevailing under heat wave conditions. In the case of the measurement campaign used to evaluate the model, the modelled heat flux represents 20% of the overall cooling flux ($Q_{wat-pav}$ +LE) due to the pavement watering.

The latent heat flux is limited by the water holding capacity of the pavement. This important parameter has been estimated using two methods: one based on simulation and the other based on the observation. The results are almost similar: the water holding capacity of the studied pavement is about 0.8 mm, comparable to the 1 mm height found in the literature. The estimated latent heat flux is in average 12% higher than the observed one. The relative error never exceeds 30%. An explanation of this overestimation is that the relative humidity data used for the latent heat flux calculation was probably lower than the reality (the sensor was located outside the watered area).

The global accuracy of the model was evaluated using the temperature observed at the surface and at several depths. The absolute RMSE for the surface temperature is larger when watering events are simulated (1.04^{o}C) than under dry conditions when only the soil model is used (0.71^{o}C).

The sensitivity of the model due to the node distribution has finally been

studied. Three soil model node distributions were compared. The 8/10/4 grid has almost no effect on the simulation performances (the RMSE increase is lower than 4%).

This paper provides a detail evaluation of the watering model performances when compared with experimental data. This model can be used to assess the cooling induced by pavement watering mitigation technique at micro-scale, which was not possible until now. The impact on local comfort could then be estimated.

The efficiency of watering techniques is constrained by the surface potential evaporation which depends directly on the surface holding capacity. The model could then be used to optimize the watering scenario according to the surface characteristics of street. The impact of different materials on microclimat model could then be compared as porous surface.

Acknowledgements

This research work was carried out within the scope of the EVA Project, funded by the ADEME (French Environment and Energy Management Agency) under contract no. 1216C0037 and conducted in collaboration with Veolia 2EI. The authors are grateful to the ADEME for its financial support, as well as to IFSTTAR, LHEEA, and ONEVU for providing us with the experimental data.

References

[1] J.-M. Robine, S. L. K. Cheung, S. Le Roy, H. Van Oyen, C. Griffiths, J.-P. Michel, F. R. Herrmann, Death toll exceeded 70,000 in europe during the summer of 2003, Comptes rendus biologies 331 (2008) 171–178.

[2] K. Laaidi, A. Zeghnoun, B. Dousset, P. Bretin, S. Vandentorren, E. Giraudet, P. Beaudeau, The impact of heat islands on mortality in paris during the august 2003 heat wave, Environmental health perspectives 120 (2012) 254.

[3] S. Conti, P. Meli, G. Minelli, R. Solimini, V. Toccaceli, M. Vichi, C. Beltrano, L. Perini, Epidemiologic study of mortality during the summer 2003 heat wave in italy, Environmental research 98 (2005) 390–399.

[4] M. Santamouris, L. Ding, F. Fiorito, P. Oldfield, P. Osmond, R. Paolini, D. Prasad, A. Synnefa, Passive and active cooling for the outdoor built environment–analysis and assessment of the cooling potential of mitigation technologies using performance data from 220 large scale projects, Solar Energy (2016).

[5] M. A. Hendel, M. Colombert, Y. Diab, L. Royon, Measurement of the cooling efficiency of pavement-watering as an urban heat island mitigation technique, Journal of Sustainable Development of Energy, Water and Environment Systems 3 (2015) 1–11.

[6] S. Himeno, R. Takahashi, A. Asakura, K. Koike, S. Fujita, Using snow melting pipes to verify the water sprinkling s effect over a wide area, NOVATECH 2010 (2010).

[7] M. Hendel, M. Colombert, Y. Diab, L. Royon, An analysis of pavement heat flux to optimize the water efficiency of a pavement-watering method, Applied Thermal Engineering 78 (2015) 658–669.

[8] A. M. Broadbent, A. M. Coutts, N. J. Tapper, M. Demuzere, The cooling effect of irrigation on urban microclimate during heatwave conditions, Urban Climate (2017).

[9] M. Daniel, A. Lemonsu, V. Viguié, Role of watering practices in large-scale urban planning strategies to face the heat-wave risk in future climate, Urban Climate (2016).

[10] S. Grossman-Clarke, J. A. Zehnder, T. Loridan, C. S. B. Grimmond, Contribution of land use changes to near-surface air temperatures during recent summer extreme heat events in the phoenix metropolitan area, Journal of Applied Meteorology and Climatology 49 (2010) 1649–1664.

[11] C. Grimmond, M. Blackett, M. Best, J. Barlow, J. Baik, S. Belcher, S. Bohnenstengel, I. Calmet, F. Chen, A. Dandou, et al., The international urban energy balance models comparison project: first results from phase 1, Journal of applied meteorology and climatology 49 (2010) 1268–1292.

[12] V. Masson, A physically-based scheme for the urban energy budget in atmospheric models, Boundary-layer meteorology 94 (2000) 357–397.

[13] L. Malys, Évaluation des impacts directs et indirects des façades et des toitures végétales sur le comportement thermique des bâtiments, Ph.D. thesis, École nationale supérieure d'architecture (Nantes), 2012.

[14] M. Musy, L. Malys, B. Morille, C. Inard, The use of solene-microclimat model to assess adaptation strategies at the district scale, Urban Climate 14 (2015) 213–223.

[15] J. Bouyer, Modelisation et simulation des microclimats urbains-Etude de l'impact de l'amenagement urbain sur les consommations energetiques des batiments, Ph.D. thesis, Universite de Nantes, 2009.

[16] M.-H. Azam, B. Morille, J. Bernard, M. Musy, F. Rodriguez, A new urban soil model for solene-microclimat: Review, sensitivity analysis and validation on a car park, Urban Climate (2017).

[17] S. Dupont, P. G. Mestayer, E. Guilloteau, E. Berthier, H. Andrieu, Parameterization of the urban water budget with the submesoscale soil model, Journal of Applied Meteorology and Climatology 45 (2006) 624–648.

[18] W. R. Herb, B. Janke, O. Mohseni, H. G. Stefan, Ground surface temperature simulation for different land covers, Journal of Hydrology 356 (2008) 327–343.

[19] V. Singh, C. Xu, Evaluation and generalization of 13 mass-transfer equations for determining free water evaporation, Hydrological Processes 11 (1997) 311–323.

[20] C.-Y. Xu, V. Singh, Evaluation and generalization of temperature-based methods for calculating evaporation, Hydrological processes 15 (2001) 305–319.

[21] T. Asaeda, V. T. Ca, The subsurface transport of heat and moisture and its effect on the environment: a numerical model, Boundary-Layer Meteorology 65 (1993) 159–179.

[22] Z. Qin, P. Berliner, A. Karnieli, Numerical solution of a complete surface energy balance model for simulation of heat fluxes and surface temperature under bare soil environment, Applied mathematics and computation 130 (2002) 171–200.

[23] H. Saito, J. Simunek, Effects of meteorological models on the solution of the surface energy balance and soil temperature variations in bare soils, Journal of Hydrology 373 (2009) 545–561.

[24] M. Best, A model to predict surface temperatures, Boundary-Layer Meteorology 88 (1998) 279–306.

[25] G. Mihalakakou, M. Santamouris, J. Lewis, D. Asimakopoulos, On the application of the energy balance equation to predict ground temperature profiles, Solar Energy 60 (1997) 181–190.

[26] O. A. Alduchov, R. E. Eskridge, Improved magnus form approximation of saturation vapor pressure, Journal of Applied Meteorology 35 (1996) 601–609.

[27] J. Cohard, J. Rosant, F. Rodriguez, H. Andrieu, P. Mestayer, P. Guillevic, Energy and water budgets of asphalt concrete pavement under simulated rain events, Urban Climate (2017).